AGU PUBLICATIONS

Geophysical Research Letters

RESEARCH LETTER
10.1002/2017GL076375

Key Points:
- Precipitation variance and extreme precipitation frequency are linearly related to mean minus critical precipitable water (PW)
- Because of non-linearity, the difference between the mean PW and critical PW is very sensitive to cloud microphysical parameters
- These findings are used to show that observed precipitation statistics could be used to directly constrain model microphysical parameters

Supporting Information:
- Supporting Information S1

Correspondence to:
S. Hagos,
samson.hagos@pnnl.gov

Citation:
Hagos, S., Ruby Leung, L., Zhao, C., Feng, Z., & Sakaguchi, K. (2018). How do microphysical processes influence large-scale precipitation variability and extremes? *Geophysical Research Letters*, *45*, 1661–1667. https://doi.org/10.1002/2017GL076375

Received 15 NOV 2017
Accepted 17 JAN 2018
Accepted article online 24 JAN 2018
Published online 10 FEB 2018
Corrected 1 JUN 2018

The copyright line for this article was changed on 1 JUN 2018 after original online publication.

How Do Microphysical Processes Influence Large-Scale Precipitation Variability and Extremes?

Samson Hagos[1], L. Ruby Leung[1], Chun Zhao[2], Zhe Feng[1], and Koichi Sakaguchi[1]

[1]Pacific Northwest National Laboratory, Richland, WA, [2]School of Earth and Space Sciences, University of Science and Technology of China, Hefei, Anhui, China

Abstract Convection permitting simulations using the Model for Prediction Across Scales-Atmosphere (MPAS-A) are used to examine how microphysical processes affect large-scale precipitation variability and extremes. An episode of the Madden-Julian Oscillation is simulated using MPAS-A with a refined region at 4-km grid spacing over the Indian Ocean. It is shown that cloud microphysical processes regulate the precipitable water (*PW*) statistics. Because of the non-linear relationship between precipitation and *PW*, *PW* exceeding a certain critical value (PW_{cr}) contributes disproportionately to precipitation variability. However, the frequency of *PW* exceeding PW_{cr} decreases rapidly with *PW*, so changes in microphysical processes that shift the column *PW* statistics relative to PW_{cr} even slightly have large impacts on precipitation variability. Furthermore, precipitation variance and extreme precipitation frequency are approximately linearly related to the difference between the mean and critical *PW* values. Thus observed precipitation statistics could be used to directly constrain model microphysical parameters as this study demonstrates using radar observations from DYNAMO field campaign.

Plain Language Summary Because of nonlinearity and the broad range of scales involved, understanding the process through which in-cloud processes influences large-scale precipitation variability and extremes has been challenging. Through high-resolution modeling and theoretical/statistical analysis, this study reveals a direct link between frequency of precipitation extremes and these in-cloud processes. An application of the findings of this study for estimating important but difficult to observe in-cloud parameters is demonstrated using radar observations of rainfall statistics.

1. Introduction

The rapid expansion of computational resources is gradually making convection permitting (sub 10 km grid spacing) climate modeling a reality. Convection permitting models can potentially simulate precipitation features responsible for much of the observed precipitation variability and extremes, albeit imperfectly because of limitations in their physics parameterizations (Miura et al., 2007; Miyakawa et al., 2014; Satoh et al., 2008). This has brought the need for understanding and parameterizing cloud microphysical processes and their interactions with the large-scale dynamics to the forefront of climate modeling research. Traditionally, studies of microphysical processes and their influence on precipitation have focused on idealized limited area cloud resolving and large-eddy simulations (LESs) or realistic cases investigating the morphology (e.g., updraft intensity, stratiform rain area etc.) of some well-observed rain events. In such context, several studies have shown that surface precipitation is sensitive to the representation of different microphysical processes and their parameter choices. For example, in radiative convective equilibrium simulations, Parodi and Emanuel (2009) showed the sensitivity of convective updraft velocity and intensity of precipitation to hydrometeor terminal velocity. On the other hand, Morrison et al. (2009) showed that differences in the rain drop size distribution parameters between one-moment and two-moment schemes influence the size of the stratiform area of a storm via changes in evaporation of rain. Yet other studies point to the treatment of graupel and hail for many of the key differences among simulations with various microphysics schemes in model inter-comparison studies (e.g., Morrison & Milbrandt, 2011; Varble et al., 2011). Furthermore the break-up of rain droplets has been found to influence the overall behavior of convective systems by increasing simulation differences in evaporation rate, and thus cold pool intensity as well as differences in latent heating and buoyancy (Fan et al., 2017; Van Weverberg et al., 2012; Varble et al., 2014).

The above studies focusing on the effects of microphysical processes on the morphology of specific storms have provided important groundwork towards development and evaluation of microphysical

Table 1
Description of model parameters that were varied in six MPAS-A convection permitting simulations

	Experiment	Description
1	HCDET	High Cloud Water Detrainment From Shallow Convection q_{crit} = 0.007kg/kg (Default).
2	LCDET	Low Cloud Water Detrainment From Shallow Convection With Doubling of q_{crit} Compared to the Default Value.
3	HEVAP	High Evaporation of Rain From Shallow Convection. All the Rain From Shallow Convection Is Allowed to Evaporate.
4	LEVAP	Low Evaporation of Rain From Shallow Convection. All the Rain From the Shallow Scheme Is Allowed to Reach the Surface.
5	HRPFV	High Rain Particle Fall Velocity. br in $V = arD^{br}$ Is Increased From 0.8 to 0.95.
6	LRPFV	Low Rain Particle Fall Velocity. br in $V = arD^{br}$ Is Reduced From 0.8 to 0.655.
7	HSPFV	High Snow Particle Fall Velocity. as in $V = asD^{bs}$ Is Increased From 11.72 to 23.44
8	LSPFV	Low Snow Particle Fall Velocity. as in $V = asD^{bs}$ Is Reduced From 11.72 to 5.86.

parameterizations appropriate for weather and climate modeling. However, the influence of microphysical processes on precipitation statistics in a large-scale context is less explored. Parodi, Foufoula-Georgiou, and Emanuel (2011), using high-resolution simulations of an atmosphere in radiative-convective equilibrium, examined the effects of raindrop terminal velocity on the statistics of precipitation. They used raindrop terminal velocity as a physical parameter to explain the statistical variability of convective rainfall over a range of scales. In the same spirit, this study examines the role of microphysical processes in the representation of precipitation variability and extremes. By considering multiple microphysical parameters in realistic simulations involving a large population of convective systems, this study aims at providing a theoretical framework for interpreting the sensitivities of precipitation statistics to changes in microphysical parameters and using observations to constrain those parameters.

2. Description of Model and Simulations

The model used in this study is the Model for Prediction Across Scales-Atmosphere (MPAS-A) (Hagos et al., 2013; Skamarock et al., 2012). This non-hydrostatic global variable resolution model formulated on an unstructured grid allows grid refinement in certain regions of interest. In this study, a high-resolution region at 4 km grid spacing is centered over the equatorial Indian Ocean and covers much of the Indian Ocean (Figure S1 in the supplementary material) in a global model domain that uses a 32 km grid-spacing globally, with a gradual transition between the two resolutions. In order to assess the sensitivities of precipitation to microphysical parameters, eight simulations are performed. The simulations differ by the values of parameters in the shallow convection or cloud microphysics scheme. A total of four parameters are perturbed. The first two parameters are in the University of Washington shallow convection scheme (Park & Bretherton, 2009). The parameters control the detrainment of condensate and evaporation of rain, respectively. The other two parameters are in the Morrison and Gettelman (2008) microphysics scheme and they control raindrop fall velocity and snow particle fall velocity, respectively. A brief description of the simulations is given in Table 1. The microphysical parameter changes are designed to introduce a significant degree of sensitivity while maintaining the realism of the simulations. Each simulation is run for 12 days starting on November 15, 2011 and initialized from the ERA-Interim reanalysis (Dee et al., 2011). The period covers a suppressed and an active phase of an MJO episode observed over the equatorial Indian Ocean during the DYNAMO field campaign (Yoneyama et al., 2013). This MJO case is selected because of the availability of radar observed precipitation statistics from the field campaign. Specifically precipitation from the S-POL radar located at the Maldives' atoll of Addu and a C-band radar aboard the R/V Revelle are averaged into hourly 30 km grid for comparison with the simulations in this study.

The precipitation and precipitable water from the refined region at 4 km grid spacing are regridded to an analysis domain with 30 km grid spacing, within a 40° longitude by 20° latitude box centered at 73°E and the equator (Figure S1). Hereafter the analysis domain refers to all the values in the three dimensional data corresponding to the 12 day long hourly values in this rectangular area. The performance of each simulation in capturing the observed evolution of MJO precipitation is shown in Figure S2.

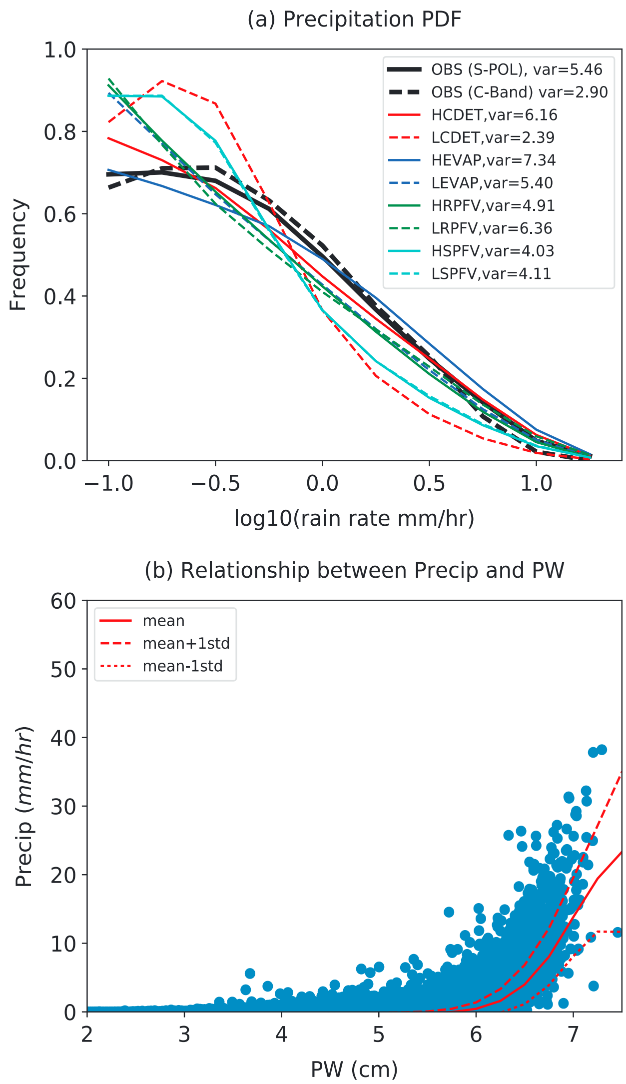

Figure 1. (a) PDF of rainrate From the MPAS-A simulations and (b) the relationship Between pre- cipitation rate and precipitable water (cm) for one of the simulations. The dots represent hourly precipitation and precipitable water. The solid red line marks the mean and the dashed lines mark +/− standard deviation.

3. Impacts of Microphysics on Variance and Extremes of Precipitation

In order to assess how microphysics influences precipitation variance and extremes (defined here as 95th percentile of precipitation rate), we perform analysis of the simulations and present statistical and theoretical considerations in parallel. We start by examining the distribution of hourly precipitation intensities and variances. Figure 1a shows the logarithmic probability distribution of hourly precipitation intensities for the 8 simulations and observations. The precipitation variances calculated over the analysis domain are provided in the legends and range from 2.39 to 7.34 (mm hr^{-1})^2 among the simulations and those from the DYNAMO observations are 2.90 and 5.46 (mm hr^{-1})^2. In general, microphysical changes such as reduction of raindrop and snow particle fall speed in the microphysics scheme, and enhanced cloud water detrainment and enhanced evaporation of raindrops in the shallow convection scheme all lead to increased precipitation variance and increased frequency of extreme precipitation to various extents.

We consider the well-documented relationship between precipitation and precipitable water (Ahmed & Schumacher, 2015; Bretherton, Peters, & Back, 2004; Holloway & Neelin, 2009). That is, on average, precipitation gradually increases with precipitable water up to a critical point beyond which it increases rapidly. This relationship has been used as a metric for evaluating climate models such as their performance in simulating the Madden-Julian Oscillation (Kim et al., 2014).

This is shown in Figure 1b for one of the simulations. The dots in the scatter plot represent hourly mean precipitation and precipitable water at each grid point of the analysis domain. In this specific case, the mean precipitation is shown to pick up rapidly at precipitable water value of about 6 cm. An often overlooked feature of this relationship is that the precipitation variance for each precipitable water bin also increases non-linearly with the precipitable water in a manner similar to that of the mean precipitation. This is demonstrated in Figure 1b in which the standard deviation shown by the difference between the dotted or dashed lines and the solid line also increases with precipitable water. This has important implications for the overall precipitation variance and the probability of extreme precipitation.

To understand the implications of the non-linear behavior of precipitation on the variance and extremes, consider the total variance of hourly precipitation over the analysis domain (hereafter referred to as domain variance var_d).

$$\mathrm{var}_d = \frac{1}{N}\sum_{i=1}^{N}\left(p_i{}^2\right) \tag{1}$$

where N is the total number of hourly data points in the analysis domain, which is a product of the number of hourly precipitation values in the 12 days and the number of grid points in the area under consideration, and p_i is the deviation of each sample point from the mean of the set of N points.

Now consider an arbitrary precipitable water bin k that contains n_k hourly precipitation values corresponding to the precipitable water values between PW_k and PW_{k+1}, with bin averaged deviation from

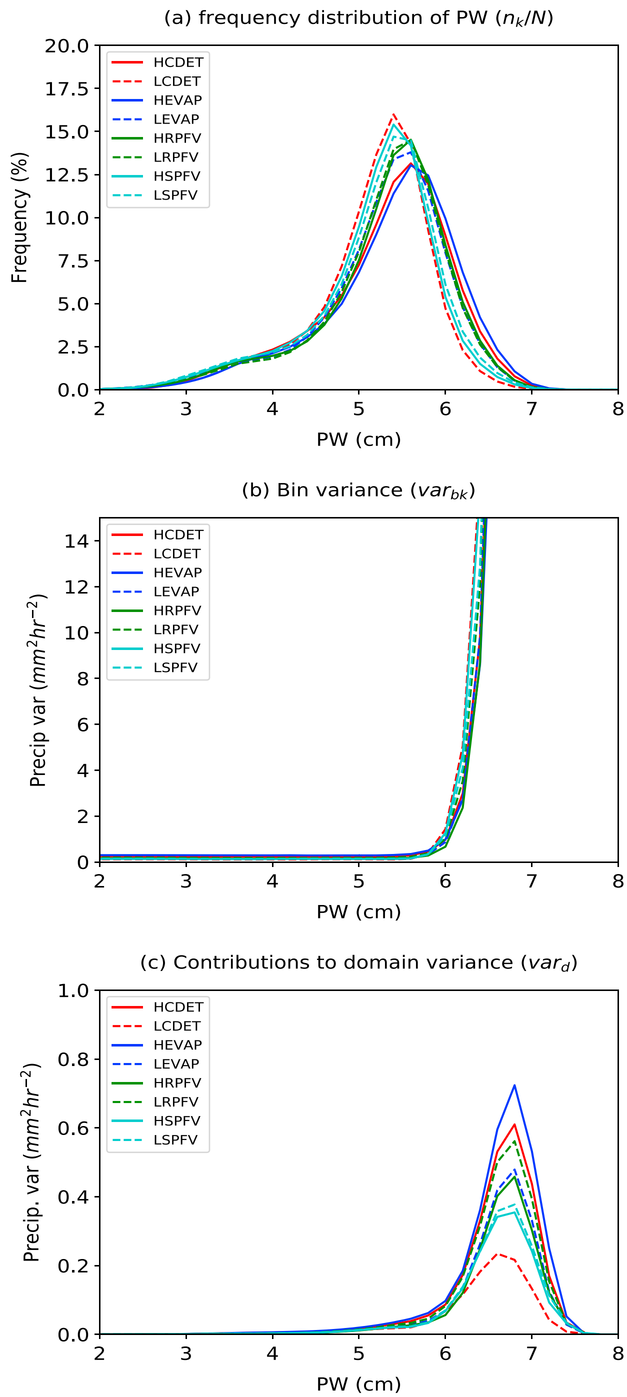

Figure 2. (a) Frequency distribution precipitable water, (b) the relationship Between local precipita- tion variance ($mm^{2}\ hr^{-2}$) vs precipitable water (mm) and (c) the contribution of each precipitable water bin to the total precipitation variance.

the mean, $\overline{p}_k$. We define the deviation of precipitation of point j from this bin averaged deviation as p_{jk} such that $p_i = \overline{p}_k + p_{jk}$.

Equation (1) can then be rewritten as

$$\mathrm{var}_d = \frac{1}{N}\sum_{k=1}^{n_b}\left[\sum_{j=1}^{n_k} p^2{}_{jk} + n_k\overline{p}_k^2\right] \tag{2}$$

where n_b is the number of precipitable water bins. After some rearrangement (2) is reduced to

$$\mathrm{var}_d = \sum_{k=1}^{n_b}\left(\frac{n_k}{N}\right)\left\{\sum_{j=1}^{n_k}\frac{p^2{}_{jk}}{n_k} + \overline{p}_k^2\right\} \tag{3}$$

The first term in the curly bracket represents the contribution from the precipitation variance within a given precipitable water bin and the second term represents the precipitation variance associated with precipitable water variability. In other words, if hourly precipitation were related only to the hourly precipitable water and no other factor, the first term would be zero and all the precipitation variance would be related to the variations in the precipitable water. For brevity the term in the curly bracket will be referred to as in-bin variance var_{bk}, which is small for k with precipitable water below some critical value, such that

$$\mathrm{var}_d = \sum_{k=kcr}^{n_b}\left(\frac{n_k}{N}\right)\mathrm{var}_{bk} \tag{4}$$

where kcr is the bin corresponding to the critical precipitable water value. Equation (4) relates the domain precipitation variance with the frequency distribution of precipitable water $\frac{n_k}{N}$ and the within-bin precipitation variance var_{bk}. According to (4), differences in microphysical parameters could introduce differences in precipitation variance and hence differences in extreme precipitation by some combination of changes in precipitable water amount and/or by differences in the way precipitation relates to precipitable water. The contributions of these two effects can then be quantified.

Figure 2 shows the precipitable water frequency distribution $\frac{n_k}{N}$ (Figure 2a), the dependence of within-bin precipitation variance var_{bk} on the precipitable water (Figure 2b), and the dependence of the domain precipitation variance var_d on the precipitable water (Figure 2c). The number of precipitable water bins is 50 and the bin sizes are 0.2 cm. As discussed above the latter is the bin-wise product of the former two. It is apparent that much of the differences in domain precipitation variance among the simulations with different microphysical parameters arise from differences in the precipitable water statistics (Figure 2a). The within-bin precipitation variance shows little inter-simulation difference (Figure 2b). The contribution of each precipitable water bin to the domain variance in precipitation is dominated by PW values between 5.5 cm and 7.5 cm (Figure 2c). It peaks at about 6.75 cm because above 5.5 cm the precipitable water frequency decreases rapidly (Figure 2a) while the within-bin variance increases rapidly (Figure 2b).

The non-linear nature of the within-bin precipitation variance has important implications for simplifying Equation (4). First, since the within-bin variance is essentially zero below a certain threshold value of precipitable water PW_{cr}, estimated to be about 6 cm in this particular case (see Figure 2b) with a corresponding bin

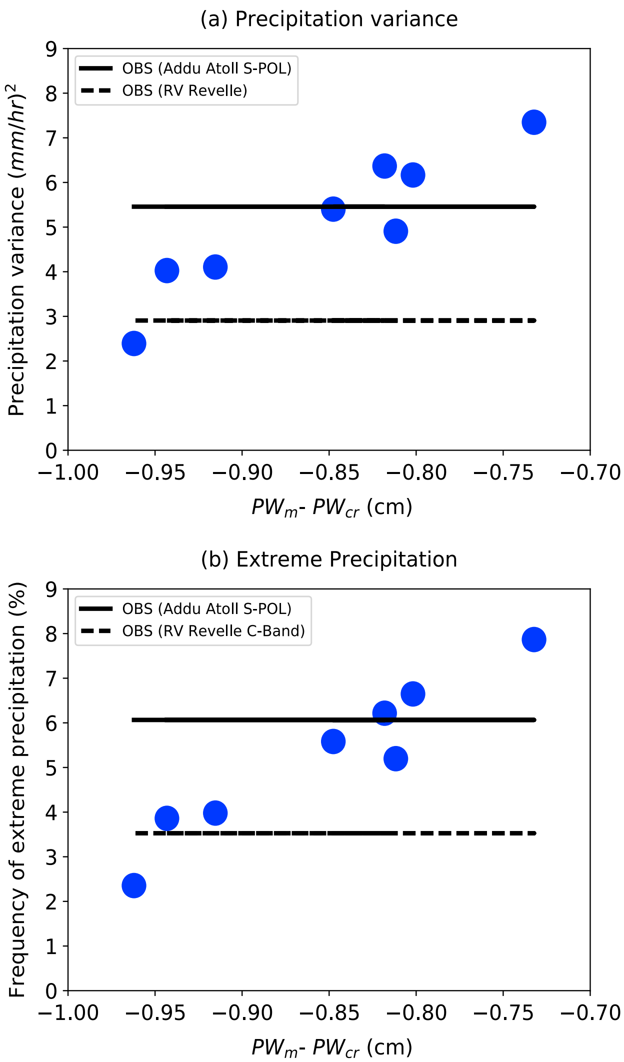

Figure 3. (a) Domain precipitation variance vs. the difference Between domain mean precipitable water and the critical precipitable water and (b) the frequency of greater than 95 percentile precipitation (%) vs. the difference Between domain mean precipitable water and the critical precipitable water (cm).

index k_{cr}, the summation can be truncated to exclude bins with index less than k_{cr}, as assumed in Equation (4). Second, beyond the critical value, the within-bin variance increases very rapidly. Therefore it is approximately independent of the precipitable water except near the critical value. Therefore Equation (4) can be further simplified to.

$$\mathrm{var}_d = \overline{\mathrm{var}_b} \sum_{k=k_{cr}}^{n_b} \left(\frac{n_k}{N}\right) \tag{5}$$

Thus the variance in precipitation is approximately a linear function of the frequency of PW above the critical value and some mean within-bin variance, $\overline{\mathrm{var}_b}$, corresponding to the average of the within-bin variance for precipitable water bins above the critical value.

There are two points to note from Figure 2a. First the frequency distribution of precipitable water is approximately Gaussian. This is expected from the Central Limit Theorem, since the sample size is large and random fluctuations dominate the precipitable water variability. Second, the differences in microphysical parameters do not significantly change the shape of the frequency distribution of precipitable water. This might be related to the relatively small magnitudes of the perturbations involved. One could imagine major changes in parameter or structural changes in the parameterizations affecting the standard deviation of the Gaussian distribution. The above two points can simplify the representation of the relationship of precipitable water statistics to variations in microphysical parameters. For brevity let us consider a continuous form of the frequency distribution that is given by a Gaussian function G centered at some mean precipitable water:

$$\sum_{k=kcr}^{n_b} \left(\frac{n_k}{N}\right) \simeq \int_{PW_{cr}}^{\infty} G(x - PW_m)dx \tag{6}$$

which can also be written as

$$\sum_{k=kcr}^{n_b} \left(\frac{n_k}{N}\right) \simeq \int_{(PW_{cr}-PW_m)}^{\infty} G(y)dy \tag{7}$$

Since G is a positive definite function, the cumulative distribution, and hence the variance is strictly increasing functions of $PW_m - PW_{cr}$. Specifically, for a Gaussian distribution the precipitation variance becomes an error function of $PW_m - PW_{cr}$, which in turn can be approximated by a linear relationship over a limited interval. Figure 3 shows that this is indeed the case. Both precipitation variance and the probability of extreme precipitation (defined as values greater than the 95$^{\text{th}}$ percentile) increase linearly with the difference between the mean and critical precipitable water contents. Thus the changes in mean precipitable water as well as the critical precipitable water due to changes in microphysical parameters are linked to the precipitation variance as well as the frequency of extreme precipitation.

This has implications for constraining model microphysical parameters and parameterizations. While the difference between mean precipitable water and critical precipitable water is difficult to observe directly, precipitation variance can be obtained from satellite, radar or rain-gauge measurements rather easily. In this specific case for example the precipitation variance and frequency of extreme precipitation from the two DYNAMO radars (Figure 3 horizontal lines) indicate that $PW_m - PW_{cr}$ values of −0.95 cm to – 0.80 cm are reasonable for capturing the observed precipitation statistics given the observational uncertainty.

4. Summary

Following the expansion of computational resources and advances in numerical methodologies, climate model resolutions are approaching convection permitting (sub 10 km) grid spacing. However, accurate depiction of extreme precipitation in convection permitting simulations requires understanding and representation of various microphysical and dynamical processes. Previous convection-permitting and LES modeling studies that examined the effect of microphysical processes on precipitation focus on their dynamic and thermodynamic effects on individual storms. Those studies have shown that microphysical processes such as evaporation associated with fall velocities of hydrometeors, particle break-up processes can modulate the evolution of storms and the precipitation associated with them. However, the cross-scale effects of microphysical processes on precipitation variability over a large population of convective clouds and therefore their impacts on the frequency of extremes have not been investigated.

In this study, global variable resolution convection-permitting model simulations are used to examine how microphysical processes influence precipitation variance and the frequency of extremes. The MPAS-A simulations of the initiation of November 2011 episode of MJO are analyzed. The high-resolution (4 km grid-spacing) region of the global MPAS-A simulations covers the equatorial Indian Ocean, with a 32 km grid spacing elsewhere. The eight simulations include variations in microphysical parameters that control cloud water detrainment and evaporation of rain from shallow clouds, and rain and snow particle fall velocity. Three key findings are noted. First, analysis of the simulations shows that the microphysical processes primarily regulate the frequency distribution of precipitable water (Figure 2a). Second, because of the non-linear relationship between precipitation and precipitable water, precipitable water values that exceed a certain critical value at which precipitation starts to rapidly increase, contribute disproportionately to the precipitation variability (Figure 2b). Third, above the critical value, the frequency distribution of precipitable water decreases rapidly (Figure 2a). Because of the above three factors, precipitation variance and frequency of extreme precipitation are very sensitive to variations in microphysical parameters. Specifically, analysis of the model simulations and theoretical considerations show that the variance of precipitation and frequency of extreme precipitation are approximately linear functions of the difference between the mean precipitable water in the domain and the value of the critical precipitable water (Figure 3).

This study also shows that the variations in microphysical parameters primarily influence the variance and extremes by shifting the frequency distribution of precipitable water relative to the critical value. The number of microphysical parameters considered in this study is limited, but one can imagine that changes in the microphysical parameters could also influence the critical value. As varying the microphysical parameters lead to a relatively wide range of $PW–PW_{cr}$ and precipitation variance as well as extreme precipitation frequency, an important implication of this study is that observed values of precipitation variance and frequency of extreme precipitation can be used to constrain microphysical parameters that are difficult to observe. As an example, for this particular case, radar observations from DYNAMO field campaign are used to estimate reasonable values for $PW–PW_{cr}$. Future studies should also explore the sensitivity of precipitation variance and extreme precipitation to other processes such as boundary layer turbulence and cloud-radiation and aerosol-cloud interactions, to better understand processes that influence convection-permitting simulations and constrain multiple parameters that dominate the fidelity of model precipitation characteristics.

Acknowledgments
This study is supported by the U.S. Department of Energy Office of Science Biological and Environmental Research (BER) as part of the Regional and Global Climate Modeling Program. Chun Zhao is supported by the "Thousand Talents Plan for Young Professionals" program of China. We acknowledge the use of computational resources of the National Energy Research Scientific Computing Center (NERSC). The Pacific Northwest National Laboratory is operated for the Department of Energy by Battelle Memorial Institute under contract DE-AC05-76RL01830. Model outputs from the convection permitting simulations are archived at NERSC. The DYNAMO legacy radar observations are supported by NSF grant AGS-1442095, and the data are archived in http://dynamo.fl-ext.ucar.edu/rsmas/dynamo_legacy/. The data from the MPAS simulations are available at https://portal.nersc.gov/project/cpmmjo/MPASMJO/.

References

Ahmed, F., & Schumacher, C. (2015). Convective and stratiform components of the precipitation-moisture relationship. *Geophysical Research Letters*, *42*, 10,453–10,462. https://doi.org/10.1002/2015GL066957

Bretherton, C. S., Peters, M. E., & Back, L. E. (2004). Relationships Between water vapor path and precipitation Over the tropical oceans. *Journal of Climate*, *17*(7), 1517–1528. https://doi.org/10.1175/1520-0442(2004)017%3C1517:RBWVPA%3E2.0.CO;2

Dee, D., Uppala, S. M., Simmons, A. J., Berrisford, P., Poli, P., Kobayashi, S., … Vitart, F. (2011). The ERA-interim reanalysis: Configuration and performance of the data assimilation system. *Quarterly Journal of the Royal Meteorological Society*, *137*(656), 553–597. https://doi.org/10.1002/qj.828

Fan, J., Han, B., Varble, A., Morrison, H., North, K., Kollias, P., … Wang, Y. (2017). Cloud-resolving model intercomparison of an MC3E squall line case: Part I—Convective updrafts. *Journal of Geophysical Research: Atmospheres* , *122*, 9351–9378. https://doi.org/10.1002/2017JD026622

Hagos, S., Leung, R., Rauscher, S. A., & Ringler, T. (2013). Error characteristics of two grid refinement approaches in aquaplanet simulations: MPAS-A and WRF. *Monthly Weather Review*, *141*(9), 3022–3036. https://doi.org/10.1175/MWR-D-12-00338.1

Holloway, C. E., & Neelin, J. D. (2009). Moisture vertical structure, column water vapor, and tropical deep convection. *Journal of the Atmospheric Sciences*, *66*(6), 1665–1683. https://doi.org/10.1175/2008JAS2806.1

Kim, D., Xavier, P., Maloney, E., Wheeler, M., Waliser, D., Sperber, K., … Liu, H. (2014). Process-oriented MJO simulation diagnostic: Moisture sensitivity of simulated convection. *Journal of Climate*, *27*(14), 5379–5395. https://doi.org/10.1175/JCLI-D-13-00497.1

Miura, H., Satoh, M., Nasuno, T., Noda, A. T., & Oouchi, K. (2007). A madden-Julian oscillation event realistically simulated by a global cloud-resolving model. *Science*, *318*(5857), 1763–1765. https://doi.org/10.1126/science.1148443

Miyakawa, T., Satoh, M., Miura, H., Tomita, H., Yashiro, H., Noda, A. T., … Yoneyama, K. (2014). Madden–Julian oscillation prediction skill of a new-generation global model. *Nature Communications*, *5*, 3769. https://doi.org/10.1038/ncomms4769

Morrison, H., & Gettelman, A. (2008). A new two moment bulk stratiform cloud microphysics scheme in the NCAR Community atmosphere model (CAM3). Part I: Description and numerical tests. *Journal of Climate*, *21*(15), 3642–3659. https://doi.org/10.1175/2008JCLI2105.1

Morrison, H., & Milbrandt, J. (2011). Comparison of two-moment bulk microphysics schemes in idealized supercell thunderstorm simulations. *Monthly Weather Review*, *139*(4), 1103–1130. https://doi.org/10.1175/2010MWR3433.1

Morrison, H., Thompson, G., & Tatarskii, V. (2009). Impact of cloud microphysics on the development of trailing stratiform precipitation in a simulated squall line: Comparison of one- and two-moment schemes. *Monthly Weather Review*, *137*(3), 991–1007. https://doi.org/10.1175/2008MWR2556.1

Park, S., & Bretherton, C. S. (2009). The University of Washington shallow convection and moist turbulence schemes and their impact on climate simulations With the community atmosphere model. *Journal of Climate*, *22*(12), 3449–3469. https://doi.org/10.1175/2008JCLI2557.1

Parodi, A., & Emanuel, K. (2009). A theory for buoyancy and velocity scales in deep moist convection. *Journal of the Atmospheric Sciences*, *66*(11), 3449–3463. https://doi.org/10.1175/2009JAS3103.1

Parodi, A., Foufoula-Georgiou, E., & Emanuel, K. (2011). Signature of microphysics on spatial rainfall statistics. *Journal of Geophysical Research*, *116*, D14119. https://doi.org/10.1029/2010JD015124

Satoh, M., Matsuno, T., Tomita, H., Miura, H., Nasuno, T., & Iga, S. (2008). Nonhydrostatic icosahedral atmospheric model (NICAM) for global cloud resolving simulations. *Journal of Computational Physics*, *227*(7), 3486–3514. https://doi.org/10.1016/j.jcp.2007.02.006

Skamarock, W. C., Klemp, J. B., Duda, M. G., Fowler, L. D., Park, S.-H., & Ringler, T. D. (2012). A multiscale nonhydrostatic atmospheric model using centroidal Voronoi tesselations and C-grid staggering. *Monthly Weather Review*, *140*(9), 3090–3105. https://doi.org/10.1175/MWR-D-11-00215.1

Van Weverberg, K., Vogelmann, A. M., Morrison, H., & Milbrandt, J. (2012). Sensitivity of idealized squall-line simulations to the level of complexity used in two-moment bulk microphysics schemes. *Monthly Weather Review*, *140*(6), 1883–1907. https://doi.org/10.1175/MWR-D-11-00120.1

Varble, A., Fridlind, A., Zipser, E., Ackerman, A., Chaboureau, J.-P., Fan, J., … Shipway, B. (2011). Evaluation of cloud-resolving model intercomparison simulations using TWP-ICE observations. Precipitation and cloud structure. *Journal of Geophysical Research*, *116*, D12206. https://doi.org/10.1029/2010JD015180

Varble, A., Zipser, E. J., Fridlind, A. M., Zhu, P., Ackerman, A. S., Chaboureau, J.-P., … Shipway, B. (2014). Evaluation of cloud-resolving and limited area model Intercomparison simulations using TWP-ICE observations: 1. Deep convective updraft properties. *Journal of Geophysical Research: Atmospheres*, *119*, 13,891–13,918. https://doi.org/10.1002/2013JD021371

Yoneyama, K., Zhang, C., & Long, C. N. (2013). Tracking pulses of the madden–Julian oscillation. *Bulletin of the American Meteorological Society*, *94*(12), 1871–1891. https://doi.org/10.1175/BAMS-D-12-00157.1